Ion imaging study of reaction dynamics in the N+ + CH4 system

Linsen Pei and James M. Farrar

Citation: J. Chem. Phys. **137**, 154312 (2012); doi: 10.1063/1.4759265
View online: http://dx.doi.org/10.1063/1.4759265
View Table of Contents: http://jcp.aip.org/resource/1/JCPSA6/v137/i15
Published by the American Institute of Physics.

Ion imaging study of reaction dynamics in the $N^+ + CH_4$ system

Linsen Pei and James M. Farrar[a)]
Department of Chemistry, University of Rochester, Rochester, New York 14627, USA

(Received 30 July 2012; accepted 1 October 2012; published online 19 October 2012)

The velocity map ion imaging method is applied to the ion-molecule reactions of N^+ with CH_4. The velocity space images are collected at collision energies of 0.5 and 1.8 eV, providing both product kinetic energy and angular distributions for the reaction products CH_4^+, CH_3^+, and $HCNH^+$. The charge transfer process is energy resonant and occurs by long-range electron transfer that results in minimal deflection of the products. The formation of the most abundant product, CH_3^+, proceeds by dissociative charge transfer rather than hydride transfer, as reported in earlier publications. The formation of $HCNH^+$ by C–N bond formation appears to proceed by two different routes. The triplet state intermediates CH_3NH^+ and $CH_2NH_2^+$ that are formed as $N^+(^3P)$ approaches CH_4 may undergo sequential loss of two hydrogen atoms to form ground state $HCNH^+$ products on a spin-allowed pathway. However, the kinetic energy distributions for formation of $HCNH^+$ extend past the thermochemical limit to form $HCNH^+ + 2H$, implying that $HCNH^+$ may also be formed in concert with molecular hydrogen, and requiring that intersystem crossing to the singlet manifold must occur in a significant (~25%) fraction of reactive collisions. We also report GAUSSIAN G2 calculations of the energies and structures of important singlet and triplet $[CNH_4^+]$ complexes that serve as precursors to product formation. © *2012 American Institute of Physics*. [http://dx.doi.org/10.1063/1.4759265]

I. INTRODUCTION

Reaction rates and energy disposal in elementary chemical reactions play an important role in a first principles understanding of many complex chemical environments, chief among them atmospheric chemistry.[1] The sequences of reactions that lead to the equilibrium concentrations of chemical constituents of planetary atmospheres is a topic of great interest, not only for our own planet, but also for the moons of other planets in our solar system. Solar photons provide the energy source that drives much of the chemistry that takes place in the outer layers of planetary atmospheres, and because those photons often have sufficient energy to ionize primary atmospheric constituents, ion chemistry is especially important in initiating chemical reaction schemes.

The Cassini mission to Saturn[2] has focused particular attention on Titan, in large part because the density of Titan's atmosphere is of the same order of magnitude as Earth's. The primary constituents of Titan's atmosphere are nitrogen (~96%) and methane (~4%), with traces of larger hydrocarbons,[3] but the Huygens probe of Titan has revealed a far wider array of chemical reaction products. Current wisdom suggests that ion processing on Titan is initiated by the reactions of N_2^+ and N^+ ions produced by primary ionization with CH_4.[4] Because of the strength of the N–N bond in the molecular ion N_2^+, chemical reactions of this species to form carbon–nitrogen bonds are quite endoergic. However, when the primary ionization event is dissociative, forming N^+ ions, these reactants are capable of undergoing exoergic reactions that form C–N bonds.

Chemical reaction rates often depend on the internal energy distributions of reactants.[5] Because the products of one reaction serve as the reactants for a subsequent process, understanding how energy is disposed of in key chemical processes is important not only in validating models, but also in providing fundamental tests of theoretical methods. In that spirit, our laboratory has developed experimental methods for probing energy disposal in elementary chemical reactions. Understanding the dynamics of key reactions that initiate ion processing in Titan's atmosphere is one of the goals of our work.

In this paper, we present a study of the charge transfer and bond formation reactions that occur in the $N^+ + CH_4$ system:

$$N^+ + CH_4 \rightarrow N + CH_4^+ \qquad \Delta H = -1.92\,\text{eV}, \tag{1}$$

$$\rightarrow N + CH_3^+ + H \qquad \Delta H = -0.10\,\text{eV}, \tag{2}$$

$$\rightarrow HCN^+ + H + H_2 \qquad \Delta H = -1.39\,\text{eV}, \tag{3}$$

$$\rightarrow HCNH^+ + H_2 \qquad \Delta H = -8.79\,\text{eV}, \tag{4a}$$

$$\rightarrow HCNH^+ + H + H \qquad \Delta H = -4.27\text{eV}. \tag{4b}$$

Reaction exoergicities are taken from literature values for the enthalpies of formation of reactants and products. The tabulated proton affinity of HCN was employed to estimate the enthalpy of formation for $HCNH^+$.[6] The wide range of exoergicities exhibited by these reactions results in a broad variety of chemical reaction processes and dynamics, providing not only important demonstrations of experimental methodologies, but also key tests of the current level of understanding

a)Author to whom correspondence should be addressed. Electronic mail: farrar@chem.rochester.edu.

of such processes at the level of the potential surfaces controlling the reaction dynamics.

II. EXPERIMENTAL

As described in our previous paper,[7] the experiment is conducted with a crossed beam instrument equipped with a velocity map product imaging (VMI) detector.[8] The imaging system measures all product velocities for a given mass in a single detection time interval, resulting in a significant enhancement of detection efficiency owing to the intrinsic multiplex advantage of the method. The experimental method is based upon important developments from other laboratories.[9,10]

The primary ion beam is formed by electron impact[11] on a mixture of 10% N_2 in He. The primary product of electron impact on this mixture is He^+, which then reacts with N_2 to form ground state N^+ (^3P) cations by dissociative charge transfer.[12] Following extraction, mass selection, and deceleration and focusing by a series of ion optics, the continuous beam of ions is delivered to the volume defined by the repeller and extraction electrodes of a velocity map imaging detector. The ion beam has a roughly triangular kinetic energy distribution with a FWHM of approximately 0.50 eV in the laboratory frame of reference. The neutral beam is a supersonic expansion produced by a pulsed solenoid valve located 10 mm upstream from a 1 mm skimmer. The stagnation pressure of the CH_4 gas behind the 0.1 mm diameter nozzle is 3 atm, and the beam has a Mach number of ~10, corresponding to a velocity distribution with FWHM of ~6%–8%. The pressure in the collision chamber is $\sim 1 \times 10^{-6}$ Torr with the beams running.

The reactant beams intersect at the center of a collision volume defined by two circular electrodes of radius 38 mm spaced by 20 mm. The lower repeller electrode, and the upper extractor electrode are held at ground potential as the ion and neutral beams intersect. Product detection is achieved by velocity map imaging,[8] employing the two-electrode geometry described by Suits *et al.*[13] Because the reactants and products are charged, product detection must be initiated by pulsed electric fields applied to the collision volume after reaction has taken place. The detection pulses, applied to the repeller and the extractor with separate high voltage pulse generators (DEI PVX-4140, 4150), are synchronized to the arrival of the central portion of the pulsed molecular beam and have a rise time and duration of 25 ns and 1 to 2 μs, respectively, to allow all products to leave the volume between the repeller and extractor during the pulses.

To achieve delayed pulsed extraction, the voltage on the repeller plate, V_1, is typically pulsed to +2300 V, the precise value dependent on transverse velocity and the filling factor for the MCP detector. The voltage V_2 on the extraction electrode is pulsed to a value $V_2 = 0.65\ V_1$. This electrode has a 13 mm aperture. A grounded electrode with a 20 mm aperture placed 13 mm above the extraction electrode provides velocity mapping for the product ions at the imaging plane, located 0.6 m downstream from the grounded lens.

Prior to striking the imaging plane of the detector, defined by the front face of a pair of chevron-mounted microchannel plates, the ions pass through a grounded grid. The MCPs are gated by a pulse of base width 80 ns, which results in an effective "on" time of ~40 ns, allowing an equatorial slice of the product ion cloud to be recorded by the phosphor screen following the MCP anode. The light image from the phosphor screen is recorded by a CCD camera (uEye 2230), which transfers the image via a universal serial bus interface to a lab computer controlled by LabVIEW software. A typical image represents the accumulation of 5000–20 000 repetitions of the pulsed valve.

As described in our previous paper, the kinematics of resonant charge transfer between an atomic beam of Ar^+ and a neutral beam of Ar produced by supersonic expansion are employed to establish a velocity marker at thermal velocity, or 5.54×10^2 m s^{-1} under our operating conditions, corresponding to a lab energy of 0.064 eV. Coupled with direct measurement of the ion beam energy distribution, these measurements result in a velocity scale that is accurate to $\pm 0.2 \times 10^2$ m s^{-1}.

The finite thickness of the collision volume is the largest experimental contributor to velocity resolution, a factor significantly more important than beam velocity distributions or the finite width of the slicing pulse. Reaction products formed at various depths within the collision volume are accelerated to different extents and, therefore, do not satisfy a unique velocity-mapping condition. Ion optics calculations with SIMION (www.sisweb.com/simion/htm) suggest that this effect is comparable to the velocity broadening of the beams.

TABLE I. Product branching fractions.

Collision energy (eV)	CH_4^+	CH_3^+	$HCNH^+$
0.02 (thermal)	0.14	0.50	0.36
0.3	0.16	0.60	0.24
0.8	0.23	0.63	0.14
1.5	0.33	0.64	0.03
2.6	0.34	0.63	0.03

III. RESULTS AND DISCUSSION

Images with sufficient signal-to-noise ratio to extract product angular and kinetic energy distributions were collected for all reaction products except HCN^+. Product branching ratios can be determined with total signal levels well below those required for reasonable images and are reported at four collision energies in the range from 0.3 to 2.6 eV in Table I. The branching ratios show that the dominant product over the entire range of collision energies is CH_3^+, rising from 50% of the total product yield at thermal energy to a plateau slightly larger than 60% at 2.6 eV. At thermal energy, $HCNH^+$ accounts for 36% of the product yield, decreasing to only a few percent with increasing collision energy. Over the same range of energies, CH_4^+ increases from ~14% at thermal energy to a little over 30% at 2.6 eV. Product images for CH_4^+, CH_3^+, and $HCNH^+$ formation are reported at collision energies near 0.5 eV and 1.8 eV.

Figure 1 shows product images for charge transfer to form CH_4^+, dissociative charge transfer to form CH_3^+, and

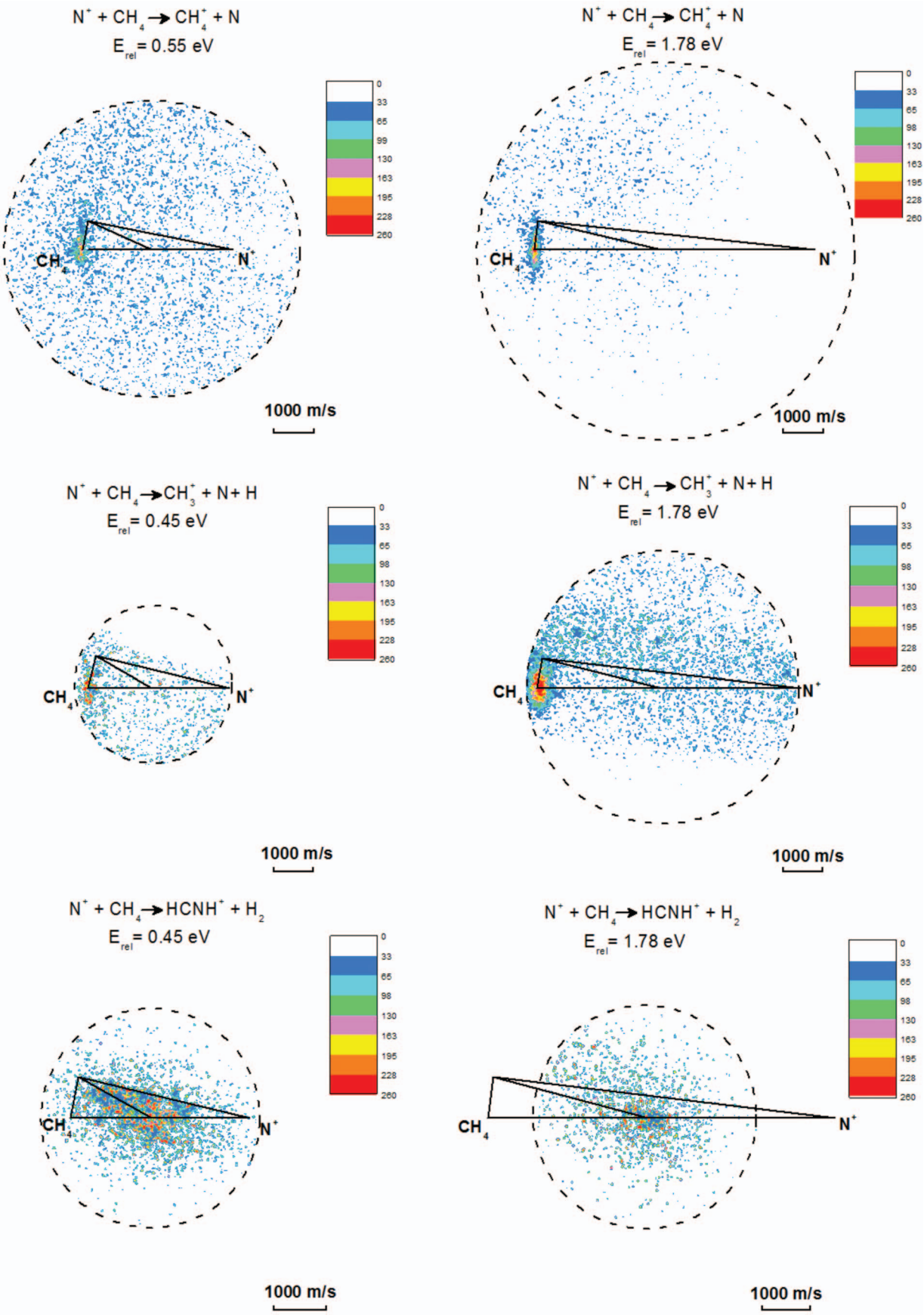

FIG. 1. Velocity space ion images for charge transfer and C–N bond formation. The images are superimposed on the appropriate kinematic Newton diagrams, and the dashed circles indicate the maximum product velocities allowed by energy conservation. Low background counts outside these circles are not shown. The left column of images corresponds to products formed at 0.5 eV, and the right column shows the same products at 1.8 eV. The top row shows images for CH_4^+; the middle row for CH_3^+; and the bottom row for $HCNH^+$.

C–N bond formation to form $HCNH^+$. The left column shows products formed at 0.5 eV and the right column shows the corresponding images at 1.8 eV. The CH_4^+ charge transfer products appear near the velocity of the incident CH_4^+ reactant, consistent with energy resonance; the CH_3^+ data have a similar appearance, consistent with the identification of these products as arising from dissociative charge transfer. The CH_3^+ images require significant background subtraction from the overlapping N^+ signal from the ion beam; this effect is especially noticeable in the low energy data, and results in a particularly weak image. The signal intensity limits the study of C–N bond formation to the dominant $HCNH^+$ channel, and the images for two collision energies are also shown in Figure 1. Although the HCN^+ images are too weak for analysis, they are centered about the collision system center of mass, similar to those for $HCNH^+$ formation.

The images represent product ion flux in laboratory Cartesian velocity coordinates[14] (v_x, v_y), and a simple velocity shift to the center of mass

$$\mathbf{u} = \mathbf{v} - \mathbf{C} \tag{5}$$

yields barycentric distributions in Cartesian coordinates, symbolized by $P(u_x, u_y)$. Barycentric recoil speed and scattering angle are given by the following expressions:

$$u = \left(u_x^2 + u_y^2\right)^{1/2}, \tag{6}$$

$$\theta = \tan^{-1}(u_y/u_x). \tag{7}$$

Because the ion and neutral beams have finite velocity widths, the transformation from laboratory to center of mass flux requires an accounting of the distribution in centroid positions (C_x, C_y) that results from the beam widths. The representation of experimental data employed in this paper is to report images like those shown in Figure 1 in raw format, as they come from the VMI detector. However, we do remove the spread in beam conditions when we extract product angular and kinetic energy distributions from the raw images, employing a grid of kinematic Newton diagrams representing the spread in experimental conditions, precisely as we have done in previous work from our laboratory that employs a rotating energy and mass analyzer.[15,16]

Product translational energy and angular distributions are extracted from the images with appropriate integrations over angle and velocity, respectively, as well as over a grid of Newton diagrams. For a given Newton diagram with index k and weight w_k, the center of mass angle and speed, θ_k and u_k, respectively, are used to construct the appropriate lab coordinates (v_x, v_y), from which the experimental intensity is registered. We employ a 5×5 grid of Newton diagrams, shown[15] to provide a thorough deconvolution of beam spreads and concomitant spreads in centroids.

The angle-averaged kinetic energy distributions are computed via Eq. (8),

$$\langle P(E_T')\rangle_\theta = \sum\nolimits_k w_k \int_0^\pi d\theta_k \sin\theta_k u_k P(u_{x,k}, u_{y,k}) \tag{8}$$

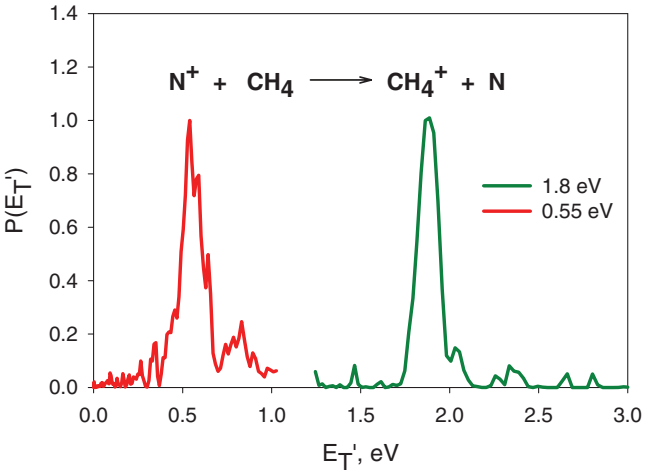

FIG. 2. CH_4^+ center of mass kinetic energy distributions for two collision energies as indicated.

and the speed-averaged angular distributions are computed in like manner from Eq. (9),

$$\langle g(\theta)\rangle_u = \sum_k w_k \int_0^\infty du_k u_k^2 P(u_{x,k}, u_{y,k}). \tag{9}$$

Integration over specific angular regions provides an assessment of the dependence of energy disposal on scattering angle. In the case of a collision complex that lives at least several rotational periods, one might expect the angular distribution to be coupled to the recoil energy distribution, especially when hydrogen atoms are ejected, but the quality of the data reported here are insufficient to justify such an analysis. The experimental data reported here illustrate a range of dynamical signatures, from direct processes with sharply peaked distributions, to examples in which the products are scattered over a broad range of angles.

The images for charge transfer in Figure 1 are extraordinarily sharp, indicative of the fact that electron transfer proceeds with minimal conversion of kinetic energy into product internal excitation, producing a relatively narrow band of product vibrational states. The image is strongly peaked in the direction of the initial velocity of CH_4, as expected in large impact parameter collisions in which the electron is transferred to the ion at long range. In Figure 2, the product kinetic energy distributions for CH_4^+ formation by charge transfer are plotted at two kinetic energies, and the corresponding angular distributions, shown in Figure 3, indicate that the CH_4^+ products are deflected minimally from the initial direction of the CH_4 precursor, revealing the signature of a direct process in which electron transfer occurs at long range.

The experimental data show clearly that the charge transfer process is energy resonant, producing very narrow product kinetic energy distributions with widths that are independent of collision energy. Energy resonance occurs when the ionization energy of the neutral reactant matches the recombination energy of the incident ion. Alternatively, that same condition is met when the kinetic energies of the approaching reactants and separating products are unchanged, and is consistent with

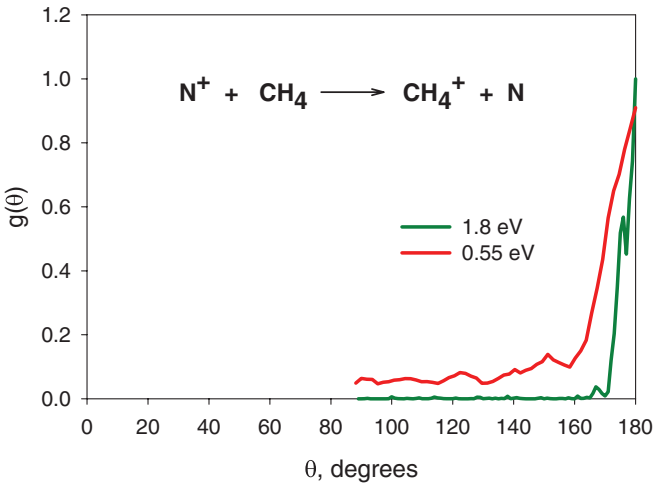

FIG. 3. CH_4^+ center of mass angular distributions for charge transfer products at two collision energies as indicated.

the negligible effect that electron transfer has on the momenta of the collision partners.

The subtler question of the role of the Franck-Condon factors for overlap of the neutral and ionic vibrational wavefunctions of the molecular collision partner requires more detailed consideration. Because the geometries of CH_4 and CH_4^+ are significantly different,[17–19] one might expect that electron transfer, like photoabsorption, is constrained by the geometry change accompanying the process. The earliest studies of charge transfer at thermal energies[20] underscore the importance of energy resonance and favorable Franck-Condon factors in determining reaction rates, but do not establish criteria that predict which effect is most important. In the present system, the charge transfer process requires crossings between potential surfaces that correspond asymptotically to $(N^+ + CH_4)$ and $(N + CH_4^+)$, and the manner in which collisions negotiate these crossings modulates the effect of favorable Franck-Condon factors. The high dimensionality of the surfaces makes a detailed quantum analysis of those crossings intractable, however.

Important insights into the interplay between energy resonance and Franck-Condon factors come from examining energy transfer studies in $H^+ + CH_4$ conducted at significantly higher collision energies than our experiments.[21] Although this system is comparable in complexity to $N^+ + CH_4$, the higher collision energies lead to important dynamical simplifications that highlight key physical ideas. The most salient experimental result is the observation that charge transfer is sharply energy resonant, but does not follow the Franck-Condon profile revealed by photoelectron spectroscopy.[22] Jahn-Teller splitting in the ground state of CH_4^+ produces a complex pattern of vibrations that is unresolved in the absorption spectrum.[19] The charge transfer experiments are conducted in an energy regime (>10 eV) in which collision times are comparable to the vibrational periods of internal motions excited by collision, leading to extensive vibronic mixing in CH_4. A relatively simple analysis, termed the internal vibronic mechanism,[21] and based on vibronic symmetry correlations and the adiabatic and non-adiabatic interactions implied by those correlations, shows that the appropriate coupling matrix elements between specific initial and final internal states are largest when the nuclear velocities remain unchanged upon electron transfer. However, the analysis of this system does not provide insight into why states with favorable Franck-Condon factors in the vicinity of energy resonance are not excited.

Like CH_4, the NH_3 molecule also undergoes a significant change in geometry upon ionization.[18] However, unlike the $N^+ + CH_4$ system, which exhibits sharp energy resonance in charge transfer but does not follow the Franck-Condon profile, the $He^{2+} + NH_3$ system[23] does exhibit a Franck-Condon distribution of NH_3^+ vibrational states. In the analysis of the results for this system, the authors focus attention on the Landau-Zener crossing probabilities between reactant and product states, showing that in the energy regime of the experiments, the characteristic time for surface crossing is shorter than characteristic vibrational periods of NH_3. This is the regime in which a Franck-Condon distribution of final states is expected and observed. Although the energy regime for our study is significantly below the energies for the systems discussed above, it is interesting to note that in both the $N^+ + CH_4$ system and the $C^+ + NH_3$ system,[7] the kinetic energy distributions for charge transfer are consistent with the higher energy experiments; i.e., both studies observe sharp energy resonance for charge transfer to CH_4, and a Franck-Condon distribution for NH_3.

The images for CH_3^+ formation in Figure 1 show a significant resemblance to those for direct charge transfer. Reaction exoergicities show that the appearance potential for CH_3^+ from CH_4^+ is 1.8 eV, slightly smaller than the exoergicity of the charge transfer reaction, indicating that even at thermal collision energies, highly excited CH_4^+ products may dissociate to CH_3^+. In previous studies of reaction rates for the formation of CH_3^+,[24–28] the accompanying neutral product has been assigned to the molecular product NH, formed by hydride abstraction, rather than N + H, the proper products for dissociative charge transfer. Although the neutral products have not been detected in any previous study of this system nor the present one, hydride abstraction, exoergic by 3.36 eV, would be expected to have dynamics distinct from charge transfer,[29,30] producing images quite different from those associated with charge transfer. The similarities of the images for CH_3^+ and CH_4^+ formation strongly suggest that CH_3^+ is formed by dissociative charge transfer.

CH_3^+ production by dissociative charge transfer is a three-body process, and the measurement of a single product momentum is insufficient to characterize the kinematics of the process completely. To extract the kinetic energy distributions shown in Figure 4, we have treated the two neutral (N, H) fragments as moving as a single assembly, thus treating the kinematics, but not the dynamics, of CH_3^+ formation like those of hydride abstraction. The kinetic energy distributions shown in Figure 4 bear a close resemblance to those for CH_4^+ formation. At both collision energies, the most probable kinetic energies of the products of dissociative charge transfer are approximately 0.2 eV below the energy resonance condition for the corresponding CH_4^+ products, as expected in a case where the speed of the heavy

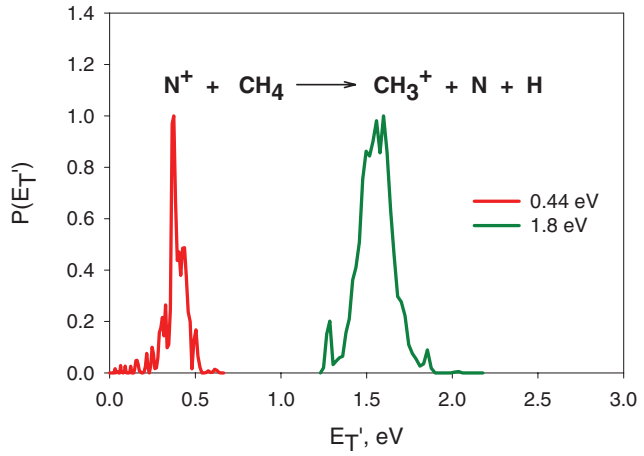

FIG. 4. CH_3^+ center of mass kinetic energy distributions for two collision energies as indicated.

fragment is unchanged relative to its precursor, but the mass is one unit smaller. Precursor internal energy must also be expended for dissociation. The widths of the distributions do broaden with increasing collision energy, indicative of the increase in total energy available for partitioning of excess energy into dissociation. The angular distributions for CH_3^+ production, obtained with the same approximate method and shown in Figure 5, are quite similar to those for CH_4^+ production. The distributions provide strong evidence that CH_3^+ is formed by dissociative charge transfer, yielding separated nitrogen and hydrogen atoms products, rather than by hydride transfer. Interestingly, the CH_3^+ yield always exceeds that of CH_4^+, suggestive of a specific dynamical mechanism rather than simple collisional dissociation of an energized precursor.

From the perspective of molecular synthesis in planetary atmospheres, the most unique chemistry associated with the $N^+ + CH_4$ system is C–N bond formation. As indicated in reactions (4a) and (4b), the strength of the C–N bond in $HCNH^+$ is sufficiently large that the ion may be formed in concert with molecular hydrogen ($\Delta H = -8.79$ eV) or two hydrogen atoms ($\Delta H = -4.27$ eV). The two different pathways have

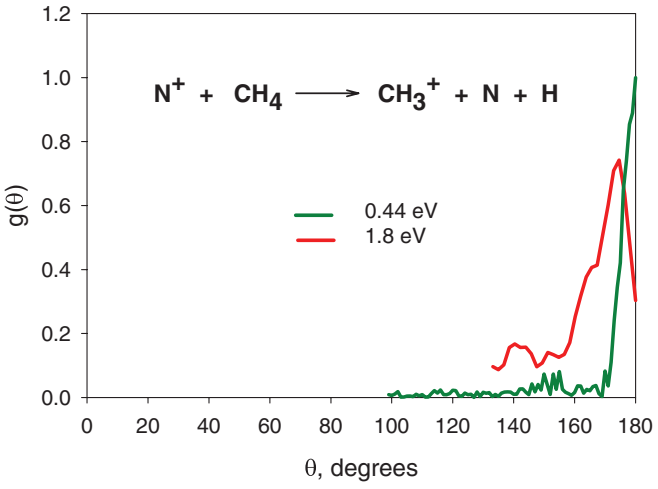

FIG. 5. CH_3^+ center of mass angular distributions for charge transfer products at two collision energies as indicated.

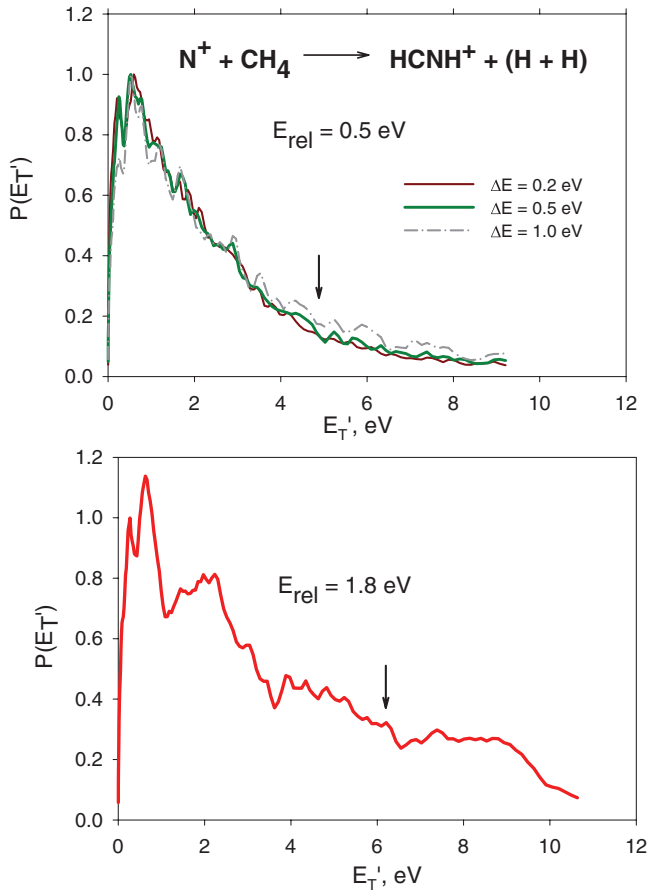

FIG. 6. (Top panel) $HCNH^+$ center of mass kinetic energy distributions at a collision energy of 0.5 eV. The thermochemical limit associated with $HCNH^+ + 2H$ is indicated with a vertical arrow. The results of deconvolution with three different ion beam energy widths are shown. The experimentally measured width is 0.5 eV. (Bottom panel) $HCNH^+$ kinetic energy distribution at 1.8 eV, deconvoluted with experimental beam energy/velocity widths. The thermochemical limit associated with $HCNH^+ + 2H$ is indicated with a vertical arrow.

important implications for energy disposal and spin conservation in the formation of $HCNH^+$. At thermal energy, extant rate data[4] show that approximately 35% of reactive collisions produce $HCNH^+$ or HCN^+. The experiments reported here indicate that the product of C–N bond formation is $HCNH^+$ in its ground electronic state, but are unable to determine from mass measurement alone whether that product is formed in concert with a hydrogen molecule or two hydrogen atoms. However, detailed analysis of the kinetic energy distributions for $HCNH^+$ formation is able to speak to this issue.

The comparison of kinetic energy release in $HCHN^+$ formation with the very different thermochemical limits associated with the H_2 or 2H products that accompany the ion is essential to discriminating between these sets of products, and requires a proper kinematic analysis, as discussed above, and summarized in Eqs. (8) and (9). The kinetic energy distributions for $HCNH^+$ formation are plotted in Figure 6. The total energies available to reaction products are given by the sum of the collision energies and the exoergicities associated with formation of $HCNH^+ + 2H$ or $HCNH^+ + H_2$. The upper panel of Figure 6 shows results for a collision energy of 0.5 eV. The maximum kinetic energy accessible to internally

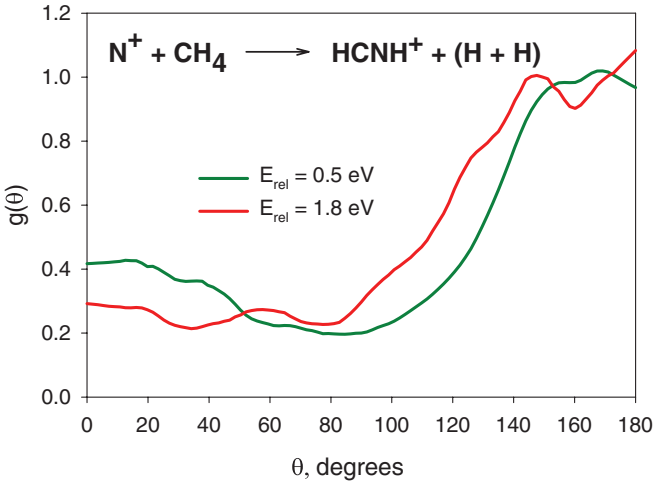

FIG. 7. $HCNH^+$ center of mass angular distributions at collision energies as indicated.

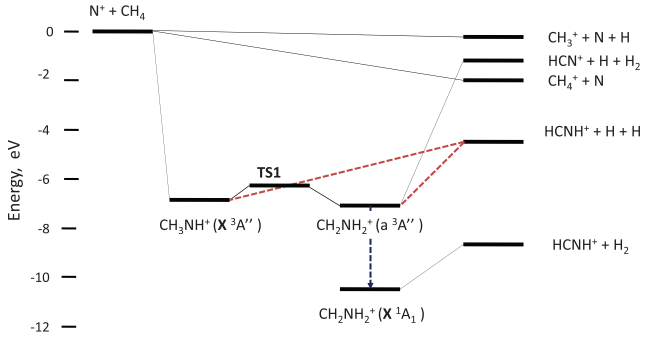

FIG. 8. Schematic reaction coordinate for production of CH_4^+, CH_3^+, and $HCNH^+$. Appropriate singlet and triplet state $[CH_4N]^+$ intermediates shown. The pathways connecting triplet state CH_3NH^+ and $CH_2NH_2^+$ intermediates, shown in red, are intended to be schematic. Details of intermediates and transition states are reported in the supplementary material. The blue dashed vertical line denotes intersystem crossing between the $a\ ^3A''$ state of $CH_2NH_2^+$ and the $\mathbf{X}\ ^1A_1$ ground state.

cold $HCNH^+$ plus two hydrogen atoms is 4.8 eV, and 9.3 eV when H_2 is formed. The experimental data show that the most probable kinetic energies of reaction products occur between 1 and 2 eV and that the majority of products are formed below the thermochemical limit for hydrogen atoms, but that a significant fraction, ~10%–15%, have kinetic energies that extend to the thermochemical limit for H_2 formation.

To demonstrate the sensitivity of the computed kinetic energy distributions to the spreads in beam energies, in the top panel of Figure 6, we have compared the results of three different kinematic calculations at the lowest collision energy, where the beams spreads are most significant in comparison with the beam energy. The benchmark calculation employs the measured FWHM value of 0.5 eV; for comparison, the plot also shows the results of energy widths of 0.2 and 1.0 eV. As expected, a larger beam energy width produces a narrower energy distribution. The comparison of the three distributions shows that the effect of beam energy spread is small. This is an especially important conclusion in evaluating kinetic energy release in the formation of $HCNH^+$, where the mass disparity between the ionic and neutral products is 28 amu vs. 2 amu, a regime where the spread in centroid positions is most severe. The kinematic calculations confirm the conclusion that a significant fraction of reaction products are formed with kinetic energies in excess of 4.8 eV, indicating that a measureable fraction of the products must be assigned to $HCNH^+ + H_2$.

The lower panel of Figure 6 reports $HCNH^+$ kinetic energy distributions at the higher collision energy, with qualitatively similar results. The thermochemical limit for $HCNH^+ + 2H$ occurs at 6.1 eV, and $HCNH^+$ products formed above this energy occur in concert with a hydrogen molecule. The fraction of products formed in this tail of the kinetic energy distribution represents ~25% of the total, a figure slightly larger than at the lower collision energy.

Product angular distributions plotted in Figure 7 show asymmetry at both collision energies, with products distributed over the full range of scattering angles. The angular distribution is skewed toward 180° slightly more at 1.8 eV than at the lower collision energy. Collision dynamics mediated by a transient complex that lives a fraction of a rotational period may produce angular distributions like those in Figure 7, but an assessment of the validity of this idea requires an understanding of the possible reaction pathways for product formation.

Central to the discussion of reaction pathways is a consideration of the multiplicities of possible products, since the reactants approach on a triplet surface, and the formation of $HCNH^+ + 2H(^2S)$ products is spin-allowed, but intersystem crossing must occur to form $HCNH^+ + H_2$ products, all of which are singlets. The kinetic energy distributions show that products formed above the thermochemical limit for $HCNH^+ + 2H$ must, therefore, be singlets, with a reaction pathway involving intersystem crossing. Hydrogen molecules may also survive at kinetic energies below this thermochemical limit if accompanying $HCNH^+$ products are internally excited. From a statistical perspective, populating the seven vibrational degrees of freedom in $HCNH^+$ but only one in H_2 makes a much larger phase space volume accessible to the ion, increasing the likelihood of forming internally excited ions, and therefore producing hydrogen molecules below the thermochemical limit. We are limited in terms of what we can say about the hydrogen products that accompany singlet $HCNH^+$ formation. The high kinetic energy products above the thermochemical limits place a lower bound, ~15 to ~25% in this study, on the fraction of products, $HCNH^+ + H_2$, that must be produced via the singlet manifold. At kinetic energies below the hydrogen atom limit, an unknown fraction of H_2 molecules or atoms could originate from products formed in the singlet manifold. However, we expect a large majority of products at kinetic energies below the hydrogen atom limit to be formed in the triplet manifold by sequential hydrogen atom ejection from triplet intermediates.

To address all of the energetic and electron spin issues associated with product formation in the $N^+ + CH_4$ system, we have constructed a schematic reaction coordinate, shown in Figure 8, for channels (1) through (4a) and (4b), using existing thermochemical data as well as the results of quantum

chemical calculations. The figure shows that the charge transfer processes forming CH_4^+ and CH_3^+ conserve spin and correlate directly with the reactants without the agency of an intermediate complex. Production of $HCNH^+$ requires the formation of C–N bonds and the migration of hydrogen atoms, a complex sequence of molecular motions most likely mediated by transient complexes. The formation of $HCNH^+ + 2H$ is exoergic by 4.29 eV, and those products are accessible with conservation of spin from the $N^+ + CH_4$ reactants. The products $HCNH^+$ and H_2 are singlet species and are not directly accessible from the triplet surface of the approaching reactants. Therefore, in constructing Figure 8, we have examined possible intermediates formed on the triplet surface of the approaching reactants, and which of those intermediates provide a pathway to the singlet manifold, yielding $HCNH^+ + H_2$ products.

In ground state $N^+(^3P)$, two of the four valence electrons are paired in a $2s$ orbital, while the remaining two electrons occupy degenerate $2p$ orbitals with the same spin, much like a triplet carbene. In analogy with carbene chemistry with unsaturated hydrocarbons,[31] in the entrance channel, the N^+ (^3P) ion may undergo a facile insertion reaction into the C–H bond of CH_4 by two mechanisms, which the present experiment cannot distinguish. Initially, the approaching reactants form an electrostatic complex, $N^+ \cdot \ CH_4$. The spin-paired $2s$ electrons may insert directly into the σ(C–H) orbital of methane to form the methylamidogen cation, CH_3NH^+, in a triplet state. Alternatively, in the $N^+ \cdot \ CH_4$ complex, N^+ may abstract a hydrogen atom from CH_4 to form a (NH^+, $\cdot CH_3$) cation-radical pair in which the unpaired electrons are born in a triplet relationship with one another. Subsequent C–N bond formation in this adduct produces triplet state CH_3NH^+. A facile 1, 2-hydrogen atom shift in CH_3NH^+ provides a plausible pathway for producing triplet state $CH_2NH_2^+$.

The first attempt to assess the structures and energies of the relevant CH_3NH^+ and $CH_2NH_2^+$ species was carried out by Dyke and co-workers[32] in photoelectron spectroscopy experiments on the two distinct radical species formed when fluorine atoms abstract a hydrogen atom from methylamine, CH_3NH_2. Quantum chemical calculations at the SCF/CI level showed that the species ionized in this experiment was a singlet aminomethyl radical, CH_2NH_2, with an adiabatic ionization potential of 6.29 eV. In conjunction with the known enthalpy of formation for CH_2NH_2, the enthalpy of formation for ground state ($\mathbf{X}\ ^1A_1$) $CH_2NH_2^+$ is 755 kJ mol^{-1}. With this information, the singlet ground state of $CH_2NH_2^+$ can be placed 1045 kJ mol^{-1}, or 10.8 eV below the ground state $N^+(^3P) + CH_4$ reactants.

Dyke and co-workers also carried out calculations at the SCF/CI level of theory to characterize the relative energies of the triplet states of CH_3NH^+ and $CH_2NH_2^+$. We have updated these calculations with GAUSSIAN calculations[33] at the G2 level of theory,[34] and report the details in the supplementary material.[35] As an internal calibration of the G2 method as applied to this system, we note that the calculated exoergicities of reactions forming ground state $CH_2NH_2^+$ and $HCNH^+$ only differ from values in standard tabulations by 0.05 and 0.10 eV, respectively.

The calculations show that the $\mathbf{X}\ ^3A''$ state of CH_3NH^+ lies 6.8 eV below the approaching reactants, and that the lowest triplet state of $CH_2NH_2^+$ ($a\ ^3A''$) lies only ~0.2 eV below the ground $\mathbf{X}\ ^3A''$ state of CH_3NH^+; the hydrogen atom migration that links these intermediates proceeds over a barrier approximately 1.3 eV in height. The calculations show pathways for sequential loss of two hydrogen atoms both from the $\mathbf{X}\ ^3A''$ state of CH_3NH^+ and the $a\ ^3A''$ state of $CH_2NH_2^+$. The pathway for sequential (1,1) hydrogen atom loss from the carbon atom of CH_3NH^+ does not have transition states with energies in excess of the total endoergicity to form $HCNH^+ + 2H$, ~2.6 eV. The pathway for sequential (1,2) hydrogen atom loss does have a barrier approximately 0.3 eV in excess of the 2.7 eV endoergicity for formation of those products. The rate-limiting step for this process represents a lower limit to the overall rate of formation of $HCNH^+ + 2H$ products: over the collision energy range from 0.5 to 1.8 eV, a Rice-Ramsperger-Kassel-Marcus (RRKM) statistical calculation[36] of this rate produces values that range from 7×10^{13} to 1×10^{14} s^{-1}. The detailed structures for all intermediates pertinent to the hydrogen atom loss pathways are reported in the supplementary material for this paper.[35]

The foregoing analysis provides a reasonable description of the spin-allowed formation of $HCNH^+$ in concert with two hydrogen atoms, representative of the significant majority of C–N reaction products. The computed lifetime for decay appears to be on the order of 10–15 fs. The rotational periods of the triplet state $CH_2NH_2^+$ or CH_3NH^+ complexes serve as an experimental "clock" for reaction. The total angular momentum of the complex can be estimated as ~60$\hbar$ by extrapolating the reported rate for reaction at thermal energy[4] to 0.5 eV and converting to a cross section. Using a moment of inertia of 3×10^{-39} g cm^2, taken from the G2 calculations, we estimate that the rotational period of the complex is approximately 300 fs, a number that should be interpreted with broad error limits. The osculating model of chemical reactions[37] that proceed through a complex that decays in a fraction of a rotational period parameterizes the angular distribution asymmetry as a function of the ratio of rotational period τ_R to lifetime τ as follows:

$$g(\pi)/g(0) = \cosh(\tau_R/2\tau). \quad (10)$$

The observed asymmetries in these experiments lie in the range from 2 to 10, corresponding to lifetimes between 0.17 τ_R and 0.4 τ_R, or 50–120 fs. Given the healthy error limits on the estimate of rotational period, the agreement between the lifetimes obtained from angular distributions and calculations is acceptable.

Although the formation of the ground state products $HCNH^+ + H_2$ is spin-forbidden, the experimental data indicate that a measurable fraction of $HCNH^+$ products must come from a spin-forbidden route. If intersystem crossing from the $a\ ^3A''$ state of $CH_2NH_2^+$ to the $\mathbf{X}\ ^1A_1$ ground state is facile as might be expected, then (1,2) elimination of H_2 from $\mathbf{X}$ state $CH_2NH_2^+$ leads to the $HCNH^+ + H_2$ products. In our hands, however, the G2 calculations for this pathway did not produce a transition state. However, the calculations did reveal a transition state for (2,2) elimination to form CH_2N^+,

a result that is not surprising because one isomeric form of $CH_2NH_2^+$ is isoelectronic with ethylene, C_2H_4, known to eliminate hydrogen both by geminal (1,1) and vicinal (1,2) elimination.[38] This product lies significantly higher in energy than $HCNH^+$, and its formation is exoergic by 5.8 eV. The kinetic energy distributions in Figure 6 extend well past the thermochemical limits that formation of CH_2N^+ dictate, requiring that a significant fraction of the products be $HCNH^+$. The calculations we have carried out, while instructive, appear to be incomplete, and warrant additional study.

The energy diagram of Figure 8 suggests that because of the larger exoergicity for forming $HCNH^+$ in concert with H_2, the rate of reaction will be significantly larger than that for producing $HCNH^+$ with hydrogen atoms. An estimate of the decay lifetime of $CH_2NH_2^+$ to $HCNH^+$ products with RRKM theory[36] using reasonable estimates of parameters for a possible transition state produces lifetimes that are less than 10^{-15} s. Lifetimes this short call the validity of the statistical approximation central to RRKM theory into question. Such lifetimes are also more characteristic of "direct" reactions that produce highly asymmetric angular distributions. While the dynamics of these more highly energized molecules are undoubtedly interesting, the angular distributions of Figure 7 are already significantly asymmetric, and do not allow ready identification of a small fraction of products that may be produced on a much shorter timescale.

IV. CONCLUSIONS

The present study on the $N^+ + CH_4$ system has provided results on both charge transfer and the C–N bond formation condensation reaction. Charge transfer has been shown to be a sharply energy resonant process, but products in the vicinity of energy resonance with favorable Franck-Condon factors are not excited. The formation of CH_3^+ appears to occur by dissociative charge transfer, rather than hydride abstraction by N^+ from CH_4.

The formation of $HCNH^+$ clearly takes place both on triplet and singlet potential energy surfaces. $HCNH^+$ formation appears to be initiated by $N^+(^3P)$ insertion into a C–H bond to yield the triplet state CH_3NH^+ species. Hydrogen atom migration yields a second triplet species, $CH_2NH_2^+$, and both of these triplet species may undergo rapid sequential hydrogen atom loss to form ground state $HCNH^+$ via spin-allowed pathways. However, the kinetic energy distributions provide clear evidence that a significant fraction of products, up to ~25%, must form molecular hydrogen in concert with $HCNH^+$. Rapid intersystem crossing to the ground state of singlet $CH_2NH_2^+$, a species known from photoelectron spectroscopy, serves as a plausible pathway to $HCNH^+$ products formed in concert with H_2.

The possibility of conducting studies that detect hydrogen atoms formed in the C–N bond formation process, as well as a more complete theoretical understanding of the role of electron spin in $HCNH^+$ formation would be welcome outcomes of this work. We also hope that the present study will be useful not only for a more comprehensive understanding of atmospheric dynamics, but will also stimulate theoretical work that extends our knowledge of charge transfer as well as unimolecular decay in the regime in which the transition to direct dynamics occurs.

ACKNOWLEDGMENTS

The authors acknowledge support for this work under National Science Foundation Grant No. CHE-1012303.

[1] A. G. Suits, J. Phys. Chem. A **113**, 11097 (2009); D. G. Torr, Rev. Geophys. **17**, 510, doi:10.1029/RG017i004p00510 (1979).
[2] See http://saturn.jpl.nasa.gov/ for a comprehensive overview.
[3] M. Fulchignoni, F. Ferri, F. Angrilli, A. J. Ball, and A. Bar-Nun, Nature (London) **438**, 785 (2005).
[4] M. J. McEwan and V. G. Anicich, Mass Spectrom. Rev. **26**, 281 (2007).
[5] W. A. Chupka and M. E. Russell, J. Chem. Phys. **48**, 1527 (1968); **49**, 5426 (1968).
[6] See http://webbook.nist.gov/chemistry/ for thermodynamic parameters.
[7] L. Pei and J. M. Farrar, J. Chem. Phys. **136**, 204305 (2012).
[8] A. Eppink and D. H. Parker, Rev. Sci. Instrum. **68**, 3477 (1997).
[9] E. L. Reichert, S. S. Yi, and J. C. Weisshaar, Int. J. Mass Spectrom. **196**, 55 (2000); E. L. Reichert, G. Thurau, and J. C. Weisshaar, J. Chem. Phys. **117**, 653 (2002); E. L. Reichert and J. C. Weisshaar, J. Phys. Chem. A **106**, 5563 (2002).
[10] J. Mikosch, U. Fruhling, S. Trippel, D. Schwalm, and M. Weidemuller, Phys. Chem. Chem. Phys. **8**, 2990 (2006); J. Mikosch, S. Trippel, C. Eichhorn, R. Otto, U. Lourderaj, Science **319**, 183 (2008); J. X. Zhang, J. Mikosch, S. Trippel, R. Otto, and M. Weidemuller, J. Phys. Chem. Lett. **1**, 2747 (2010).
[11] H. Udseth, C. F. Giese, and W. R. Gentry, Phys. Rev. A **8**, 2483 (1973).
[12] R. D. Smith and J. H. Futrell, J. Chem. Phys. **65**, 2574 (1976).
[13] D. Townsend, M. P. Minitti, and A. G. Suits, Rev. Sci. Instrum. **74**, 2530 (2003).
[14] R. Wolfgang and R. J. Cross, J. Phys. Chem. **73**, 743 (1969); B. Friedrich and Z. Herman, Collect. Czech. Chem. Commun. **49**, 570 (1984).
[15] R. M. Bilotta, F. N. Preuninger, and J. M. Farrar, J. Chem. Phys. **73**, 1637 (1980).
[16] P. E. Siska, J. Chem. Phys. **59**, 6052 (1973).
[17] C. A. Coulson and H. L. Strauss, Proc. R. Soc. London, Ser. A **269**, 443 (1962).
[18] D. C. Frost, C. A. McDowell, and D. A. Vroom, Can. J. Chem. **45**, 1343 (1967).
[19] R. N. Dixon, Mol. Phys. **20**, 113 (1971).
[20] J. B. Laudenslager, W. T. Huntress, and M. T. Bowers, J. Chem. Phys. **61**, 4600 (1974).
[21] Y. N. Chiu, B. Friedrich, W. Maring, G. Niedner, and M. Noll, J. Chem. Phys. **88**, 6814 (1988).
[22] J. W. Rabalais, T. Bergmark, L. O. Werme, L. Karlsson, and K. Siegbahn, Phys. Scr. **3**, 13 (1971).
[23] M. Farnik, Z. Herman, T. Ruhaltinger, and J. P. Toennies, J. Chem. Phys. **103**, 3495 (1995).
[24] W. T. Huntress and V. G. Anicich, Geophys. Res. Lett. **3**, 317, doi:10.1029/GL003i006p00317 (1976); V. G. Anicich, W. T. Huntress, and J. H. Futrell, Chem. Phys. Lett. **47**, 488 (1977).
[25] M. Tichy, A. B. Rakshit, D. G. Lister, N. D. Twiddy, and N. G. Adams, Int. J. Mass Spectrom. Ion Process. **29**, 231 (1979).
[26] N. G. Adams, D. Smith, and J. F. Paulson, J. Chem. Phys. **72**, 288 (1980).
[27] S. Dheandhanoo, R. Johnsen, and M. A. Biondi, Planet. Space Sci. **32**, 1301 (1984).
[28] J. B. Marquette, B. R. Rowe, G. Dupeyrat, and E. Roueff, Astron. Astrophys. **147**, 115 (1985); B. R. Rowe, J. B. Marquette, G. Dupeyrat, and E. E. Ferguson, Chem. Phys. Lett. **113**, 403 (1985).
[29] J. Zabka, M. Farnik, Z. Dolejsek, J. Polach, and Z. Herman, J. Phys. Chem. **99**, 15595 (1995).
[30] L. Liu, E. S. Richards, and J. M. Farrar, J. Chem. Phys. **127**, 244315 (2007).
[31] R. D. Bach, M.-D. Su, E. Aldabbagh, J. L. Andres, and H. B. Schlegel, J. Am. Chem. Soc. **115**, 10237 (1993).
[32] J. M. Dyke, E. P. F. Lee, and M. H. Z. Niavaran, Int. J. Mass Spectrom. Ion Process. **94**, 221 (1989).
[33] M. J. Frisch, G. W. Trucks, H. B. Schlegel *et al.*, GAUSSIAN 03, Gaussian, Inc., Wallingford, CT, 2004.
[34] L. A. Curtiss, K. Raghavachari, G. W. Trucks, and J. A. Pople, J. Chem. Phys. **94**, 7221 (1991).

[35]See supplementary material at http://dx.doi.org/10.1063/1.4759265 for structural parameters, vibrational frequencies, and electronic energies of all intermediates and transition states.
[36]R. A. Marcus, J. Chem. Phys. **20**, 359 (1952).
[37]M. K. Bullitt, C. H. Fisher, and J. L. Kinsey, J. Chem. Phys. **60**, 478 (1974); D. F. Varley, D. J. Levandier, and J. M. Farrar, *ibid.* **96**, 8806 (1992).
[38]J. J. Lin, C. C. Wang, Y. T. Lee, and X. Yang, J. Chem. Phys. **113**, 9668 (2000).